

tapered roller bearing, dynamic simulation, axial load force

*Róbert KOHÁR**, *Frantisek BRUMERČÍK***,
*Michal LUKÁČ****, *Aleksander NIEOCZYM*****

NUMERICAL ANALYSIS OF ROLLER BEARING

Abstract

The aim of this paper is to detail the creation of a large tapered roller bearing model with flexible body cages in the Adams program suite for subsequent dynamic analysis and to obtain information about kinematic and dynamic relationships of steel and plastic cages under various operating conditions. The bearing model was made to closely resemble its real-life counterpart, which allows us to estimate load conditions, dynamic conditions of individual bearing parts and interactions between them.

1. INTRODUCTION

Tapered roller bearings are used in shafts which sustain large axial and radial forces. To achieve high operational reliability and long lifetimes, tapered bearings have to be set with preload at the time of assembly. Preload allows to achieve required contact stress between the inner surfaces of the raceway and the rolling elements. The authors of [1] studied the effect of bearing assembly on bearing life. As input data they used bearing preload and shaft deflection angle. Simulation results were expressed in terms of bearing stiffness and distribution of contact stresses. In addition, modifications were introduced in the shape of the edge at the base of the cone [2, 3] report the results

* University of Zilina, Faculty of Mechanical Engineering, Univerzitná 1, 010 26 Žilina, Slovakia, robert.kohar@fstroj.uniza.sk

** University of Zilina, Faculty of Mechanical Engineering, Univerzitná 1, 010 26 Žilina, Slovakia, frantisek.brumercik@fstroj.uniza.sk

*** University of Zilina, Faculty of Mechanical Engineering, Univerzitná 1, 010 26 Žilina, Slovakia, michal.lukac@fstroj.uniza.sk

**** Lublin University of Technology, Faculty of Mechanical Engineering, Nadbystrzycka 36, 20–618 Lublin, Poland, a.nieoczyn@pollub.pl

of modeling of the impact of operational factors such as angular displacements of bearing races, shaft deflection, and errors during mounting of ball bearing assemblies, on service life of a tapered roller bearing. The loadings used were radial and axial forces at varying rotational speeds. These factors were shown to effect changes in contact loads and contact stresses between the rolling element and the races, which led to reduced bearing life. Additionally, an analysis was conducted of the impact of geometric errors in internal surfaces of tapered roller bearings [3] on the value of contact forces. Describes the procedures of FEM modeling of tapered roller bearings which allow to obtain contact stresses [4, 5]. That study presents models of contact stresses and methods of modeling contact discontinuities on roller and race surfaces.

Tapered roller bearings are also investigated in terms of their material properties. Describes the influence of contact stresses on fatigue spalling of bearing races, in particular pitting and flaking away of bearing material [6]. It presents the results of FEM modeling based on generating nonlinear material models, which allows to determine contact stresses. Analyzes the impact of the internal geometry and micro-geometry of the functional surfaces of raceways at the contact with the roller and their impact on internal resistance-friction of the bearing [7].

The above-mentioned studies do not take into account the impact of the bearing retainer on load bearing capacity and service life of bearings. The literature also offers no reports on interactions between the retainer and rolling elements. A bearing retainer moves in rotary motion, and errors in its manufacture affect the life of rolling elements. Another variable that could be investigated is the type of material the retainer is made of and its impact on the value of stresses on the surfaces of the rolling elements.

2. TAPERED ROLLER BEARING MODEL

Dynamic simulations of the tapered roller bearing were performed in the MSC.Adams system. A precise geometrical model of the bearing was necessary in order to perform the said simulations. The 3D model has been created based on available drawing documentation and incorporates various methods with regards to the overall model complexity. Model design was performed in Pro/Engineer Wildfire 5 (Fig. 1), which, when compared to the MSC.Adams environment, allows simpler model creation and subsequently easier bearing geometry modifications. The bearing model assembly was transformed from Pro/Engineer into Adams environment using the Parasolid file format and was further processed based on analysis requirements. The first step included material definition for individual bearing components. The bearing consisted of inner and outer ring, cage and rollers. Table 1 lists values assigned to individual parts.

Tab. 1. Material properties of individual bearing parts
[source: own study]

	Density [kg.m ⁻³]	Young modulus [MPa]	Poisson constant[-]
Inner ring	7850	202000	0.29
Outer ring	7850	202000	0.29
Roller	7850	202000	0.29
Steel cage	7850	202000	0.29
Plastic cage	1100	3000	0.42

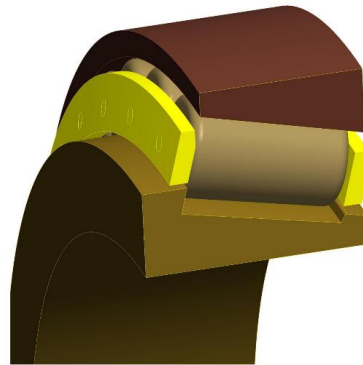


Fig. 1. Tapered roller bearing model in Pro/Engineer [source: own study]

In the next step we defined the contacts between individual bearing components. Contact type „solid to solid“ was chosen for the afore mentioned operation, defining two objects coming into contact. This was due to the geometrical complexity of the model and inability to determine all bearing parts that come into contact [8, 9]. This contact type requires the definition of the following parameters: Stiffness, Exponent, Max Damping and Penetration Distance. Contact pairs were formed between inner ring and rollers, outer ring and rollers and between ring and rollers. Parameter values for contacts of rollers with outer and inner ring have been defined based on the Hertz theory of contact pressure. We also considered a friction model based on Coulomb friction force calculation. Values of static and dynamic friction coefficient have been set according to and values of transmission velocity.

Next we defined the geometric and kinematic constraint conditions and load force. Axial load force of the outer ring was associated with „Fixed joint“ constraint, which resulted in removal of all degrees of freedom. Inner ring was associated with „Cylindrical Joint“ constraint condition, which allowed rotation and translation along the x axis. „Rotational Joint Motion“ of type „Velocity“ has been assigned to the „Cylindrical Joint“ constraint, allowing rotational movement.

This movement has been defined via the STEP function and corresponds to bearing rotational speed $n = 15.5\text{min}^{-1}$ and $n = 250\text{min}^{-1}$. Loading force was defined via gravitation acceleration „Gravity“ and „Axial Force“ of magnitude 518000 N in x axis direction, influencing the inner ring. Figure 2 shows a model with axial load force with defined geometrical and kinematic constraint conditions.

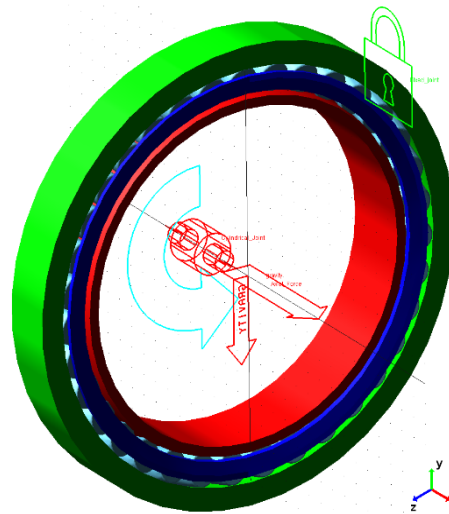


Fig. 2. Geometric and kinematic constraint conditions – axial load force [source: own study]

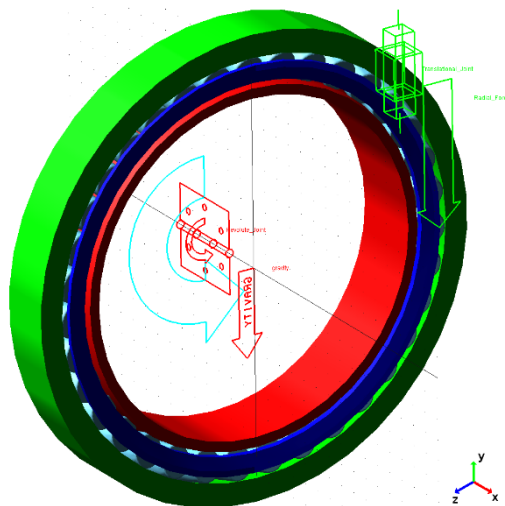


Fig. 3. Geometric and kinematic constraint conditions – radial load force [source: own study]

Constraint conditions for dynamic analysis with radial load force have been defined as following: „Revolute Joint“ has been assigned to the inner ring and allowed inner ring rotation around the x axis. „Translational Joint“ has been assigned to the outer ring, allowing movement in direction of the y axis. „Rotational Joint Motion“ of type „Velocity“ has been assigned the aforementioned constraint, allowing rotational movement. This movement has been defined in a similar fashion as described above using the STEP function. Load force was defined via gravitation acceleration „Gravity“ and „Radial Force“ of magnitude 4500000N has been applied in y axis direction, influencing the outer ring. Figure 3 shows the model under radial load force with defined geometric and kinematic constraint conditions.

After defining all constraint conditions, boundary conditions and load force, we defined the analysis type and solver parameters as follows: SIMULATE/DYNAMIC, END=30, STEPS=3000, Integrator GSTIFF, Formulation SI2, Corrector Modified, Error 1e-3, Executable External C++, Thread Count 8, Contacts Default_Library, Faceting Tolerance 1e.

3. DYNAMIC SIMULATION RESULTS – AXIAL LOAD FORCE WITH ROTATIONAL SPEED $n = 15.5$ rpm

Dynamic simulation results with axial load force and rotational speed $n = 15.5$ rpm represent force interactions between individual bearing parts, movement of bearing cage center of gravity and angular velocity thereof. Figure 4 shows forces between roller and cage, roller and inner ring and angular velocity of this roller. Maximum force between steel cage and rollers was observed during interaction of the cage with roller n.26 and is equal to 268 N (Fig. 4 up, green line). Also shown is the force between inner ring and roller n. 26 (red line), which varied between 54297 N and 59103 N, a difference of 4.2% (minimal force) and 8.1% (maximal force) when compared to theoretical calculations. The blue line displays angular velocity of roller n. 26 and varies between 483°/s and 495°/s.

Maximum force between plastic cage and rollers was observed during interaction of the cage with roller n.2 and is equal to 251N (Fig. 4 down, green line). Also shown is the force between inner ring and roller n. 2 (red line), which varied between 54467 N and 58636 N and was lower when compared to the steel cage, representing a difference of 3.9% (minimal force) and 7.1% (maximal force) when compared to theoretical calculations. The blue line displays angular velocity of roller n. 2 and varies between 483°/s and 495°/s, similar to the velocity observed for the steel cage.

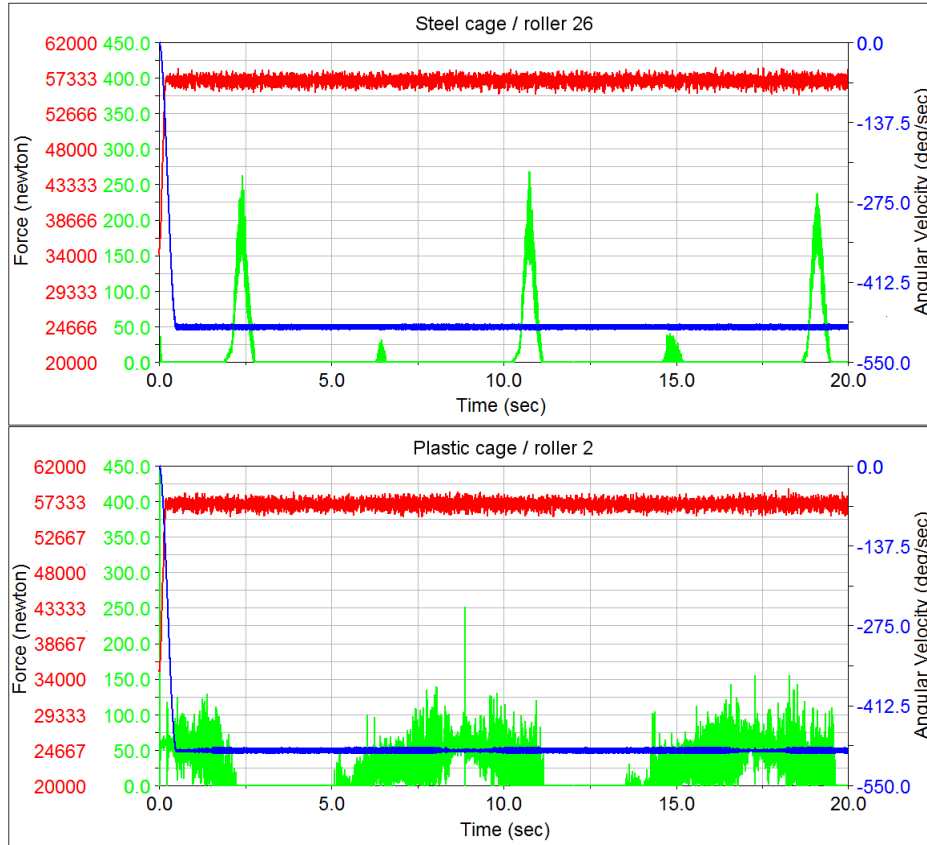


Fig. 4. Force interaction between inner ring and rollers (red lines), force interaction between cage and rollers (green lines) and angular velocity of rollers [source: own study]

Figure 5 shows the center of gravity location in the y-z plane of steel cage oriented as per Fig. 2. Figure 6 shows the center of gravity location in the y-z plane of plastic cage, fig. 7 shows force interaction between inner ring and rollers.

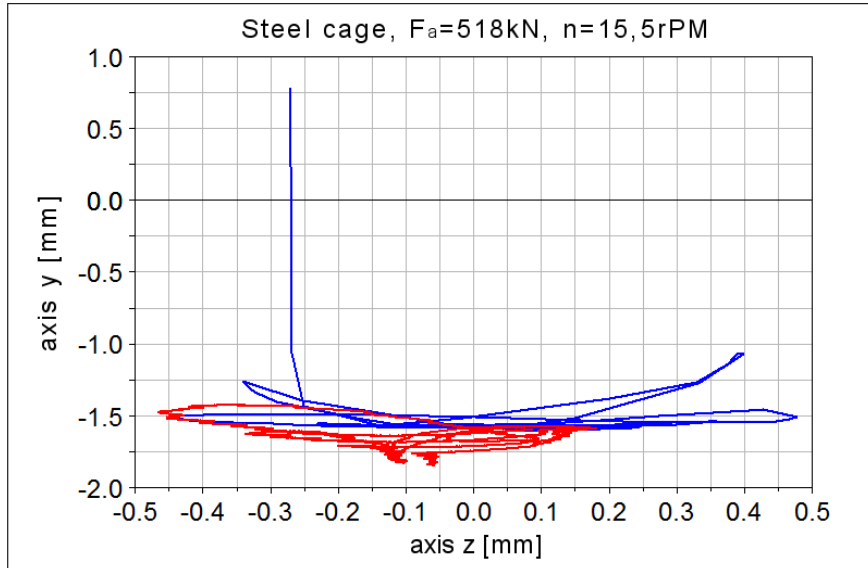


Fig. 5. Movement of center of gravity of steel cage in the y-z plane under axial load [source: own study]

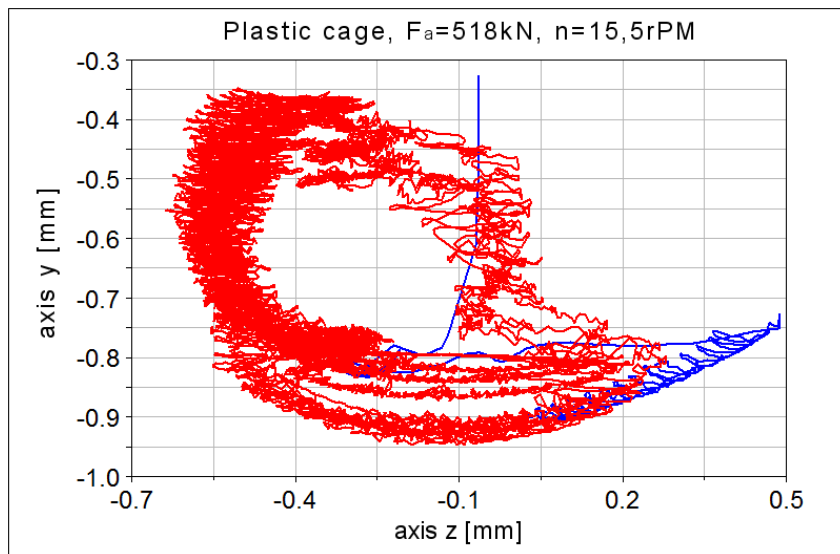


Fig. 6. Movement of center of gravity of plastic cage in the y-z plane under axial load [source: own study]

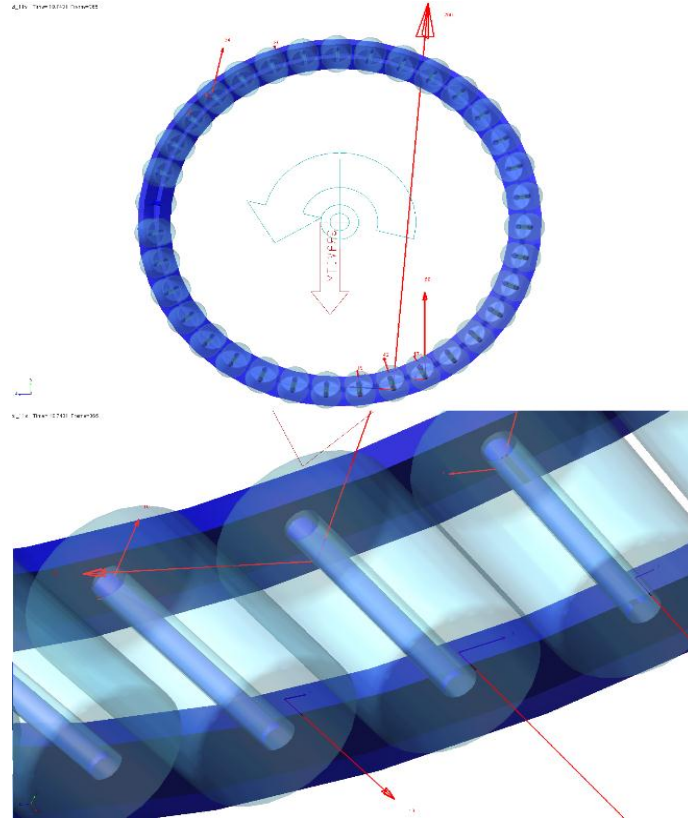


Fig. 7. Force interaction between inner ring and rollers [source: own study]

4. RADIAL LOAD FORCE WITH ROTATIONAL SPEED $n = 15.5 \text{ min}^{-1}$

Similar to axial load force, we calculated force interactions between individual bearing parts, movement of bearing cage and angular velocity thereof when subjected to radial force. Figure 8 shows force between roller and cage, roller and inner ring and angular velocity of the roller. Also shown is the force between inner ring and roller n.13 (red line). Maximum force between steel cage and rollers was observed for roller n.13 and is equal to 706N (green line). The analysis also showed that highest load rates are present at rollers 10 to 14 during start-up time (2-5 seconds) and are equal to 700N. During subsequent simulation time, the cage was in contact with rollers only when the rollers were off-loaded and maximum force value was equal to 250N. Angular speed was constant (489°/s) under applied roller load and lowered under roller load in the 20000N to 70000N range, achieving a minimum value of 445°/s (blue curve).

Figure 8 down shows force between inner ring and roller n.10 (red line) for bearing with plastic cage. Maximum force between the plastic cage and rollers was observed for roller n.10 and is equal to 670N (green line). Similar to the steel cage, highest load rates were present at rollers 10 to 14 during start-up time (2-5 seconds) and are equal to 700 N. When compared to the steel cage, the rollers were in contact not only in the off-load phase (force equal to 100 N) but also during the load phase, with the force equal to 400 N. Angular speed was constant (489°/s) under applied roller load and, similar to the steel cage, lowered under roller load in the 20000N to 70000N range, achieving a minimum value of 167°/s (blue curve) and 320°/s under load.

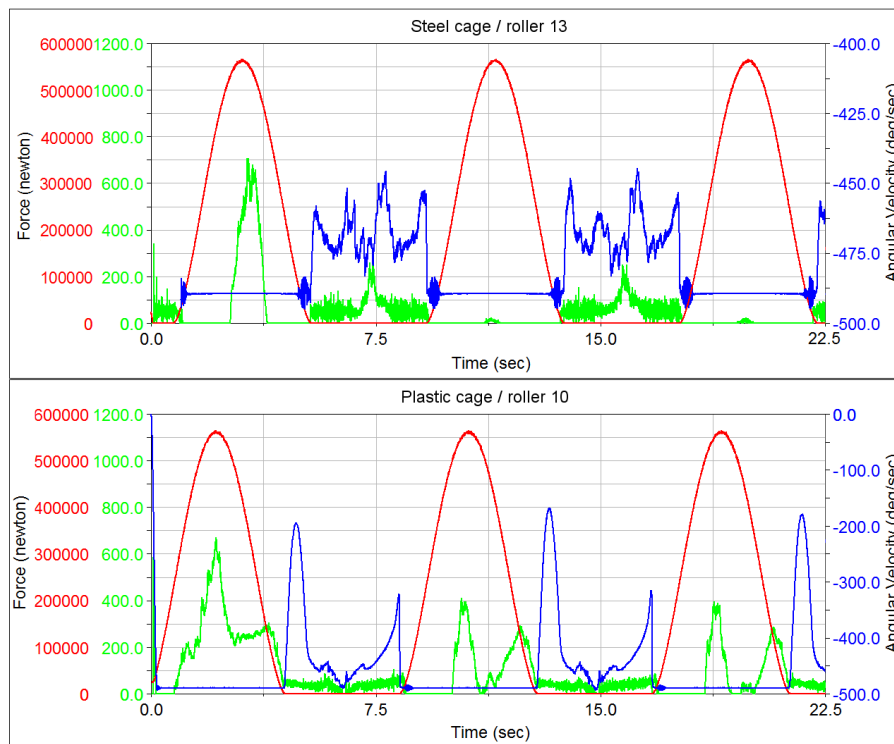


Fig. 8. Force interaction between inner ring and rollers (red lines), force interaction between cage and rollers (green lines), angular velocity of rollers (blue line) [source: own study]

Figure 9 shows the center of gravity location of the steel cage in the y-z plane, figure 10 shows the center of gravity location of the plastic cage in the y-z plane, and figure 11 shows force interaction between inner ring and rollers.

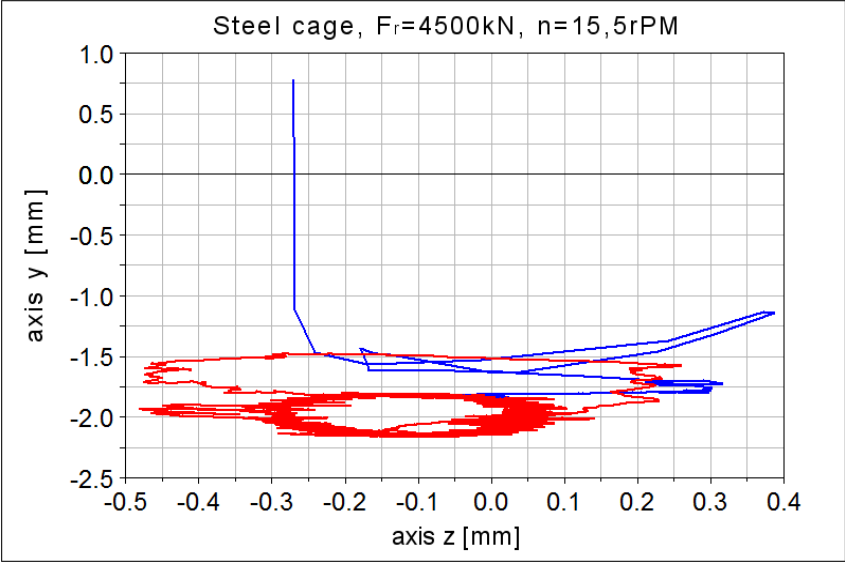


Fig. 9. Movement of center of gravity of steel cage in the y-z plane under radial load [source: own study]

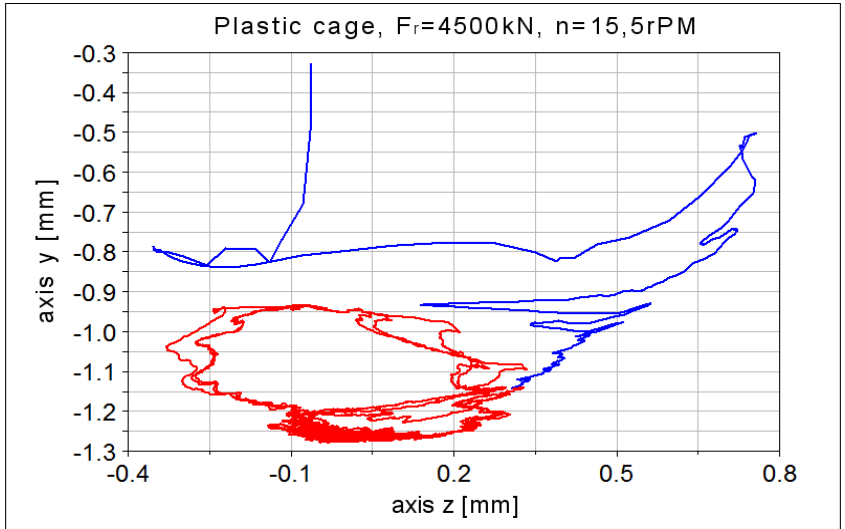


Fig. 10. Movement of center of gravity of plastic cage in the y-z plane under radial load [source: own study]

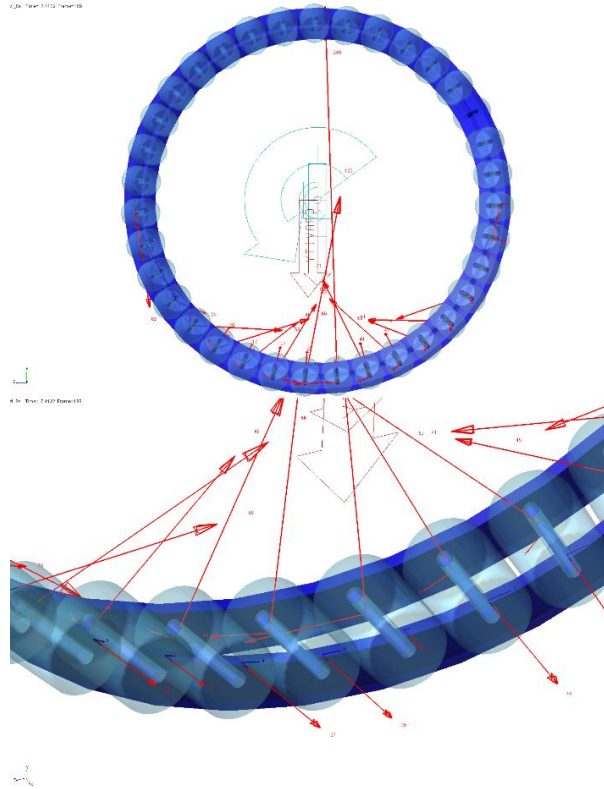


Fig. 11. Force interaction between inner ring and rollers [source: own study]

5. CONCLUSION

Based on obtained results, we can conclude that the steel cage is more appropriate for axial force load due to lower interaction force between the cage and rollers. Also reduced are bearing oscillations in both the rotation axis and in the plane normal to the said axis. Forces between rollers and bearing rings are minimally influenced by the cage type. This is also true for the angular velocity of the rollers. Radial force load results in reduced load of steel cage at lower speed, however at higher speed the plastic cage is more appropriate. At lower speed, the angular velocities of bearing rollers with steel cage are randomly changing during the offload phase and could result in undesirable behavior of the bearing. Angular velocities of plastic cage rollers exhibit a smoother behavior when compared to steel cage. Additionally, oscillations in the plane normal to the rotational axis are also lowered.

Based on the afore-mentioned results, we can conclude that the use of plastic cage is more appropriate for radial load force scenarios.

REFERENCES

- [1] VAN-CANH T., HONG S.: *Characteristics of tapered roller bearings in relation to roller profiles*. Journal of Mechanical Science and Technology, 29 (7), 2015, p. 2913–2919.
- [2] VAN-CANH T., HONG S.: *Fatigue life of tapered roller bearing subject to angular misalignment*. Proceedings of the Institution of mechanical engineers. Part C – Journal of Mechanical Engineering Science, 230 (2), 2016, p. 147–158.
- [3] VAN-CANH T., HONG S.: *Characteristics of Tapered Roller Bearing with Geometric Error*. International Journal of Precision Engineering and Manufacturing, 16 (13), 2015, p. 2709–2716.
- [4] YANG X., HUANG Q., YAN C.: *Analyzing the load distribution of four-row tapered roller bearing with Boundary Element Method*. Engineering Analysis with Boundary Elements, 56, 2015, p: 20–29.
- [5] KOHÁR R., MEDVECKÝ Š., HRČEK S.: *Usage of dynamic analysis to determine force interactions between components of rolling bearings with different rotation speed*. In: Machine Design, 4 (3), 2012, p. 145–150.
- [6] LOSTADO R., FERNANDEZ M., MAC DONALD B.: *Determination of the contact stresses in double-row tapered roller bearings using the finite element method, experimental analysis and analytical models*. Journal of Mechanical Science and Technology, 29 (11), 2015, p. 4645–4656.
- [7] JURKO J., PANDA A., VALICEK J.: *Study on cone roller bearing surface roughness improvement and the effect of surface roughness on tapered roller bearing service life* International Journal of Advanced Manufacturing Technology, 82 (5-8), 2016, p. 1099–1106.
- [8] HARRIS T. A., KOTZALAS M. N.: *Essential Concepts of Bearing Technology*. 5. edition. 2007.
- [9] GLOWACZ A.: *Diagnostics of DC and Induction Motors Based on the Analysis of Acoustic Signals*. Measurement Science Review, 14 (5), 2015, p. 257–262.